2022 IEEE Applied Power Electronics Conference and Exposition (APEC)

Modeling and Characterization of Natural-Convection Oil-Based Insulation for Medium Frequency Transformers

N. Djekanovic and D. Dujic

POWER ELECTRONICS LABORATORY
ÉCOLE POLYTECHNIQUE FÉDÉRALE DE LAUSANNE

Modeling and Characterization of Natural-Convection Oil-Based Insulation for Medium Frequency Transformers

Nikolina Djekanovic, Drazen Dujic
Power Electronics Laboratory - PEL
École Polytechnique Fédérale de Lausanne - EPFL
Lausanne CH-1015, Switzerland
nikolina.djekanovic@epfl.ch, drazen.dujic@epfl.ch

***Abstract*—Due to its high value of dielectric strength, oil is often used for transformer insulation, especially when processing high powers. Nevertheless, its presence needs to be considered when determining thermal coordination of a converter system, which also includes the challenging modeling of fluid dynamics. This paper presents an analytical model for calculation of characteristic oil temperatures for medium frequency transformers with oil-immersed windings. The characterization and verification of the developed analytical model is performed based on a small-scale experimental setup. The paper demonstrates that the analytical model reasonably agrees with the selected verification method, and can aid design optimization.**

I. Introduction

Solid state transformers (SSTs) are considered to be the key technology for future distribution grids, providing direct and alternating current interfaces for the integration of renewable energy resources and energy storages. Moreover, they are already successfully applied for traction applications, where restrictions in weight and volume exist and high conversion efficiencies are required [1], [2]. To achieve galvanic isolation between the power stages of an SST, a medium frequency transformer (MFT) is used. Nowadays, the design of MFTs is usually performed with the help of design optimization algorithms, which are built to include various transformer aspects through corresponding models. These address insulation and thermal coordination, core and winding losses, estimation of leakage and magnetizing inductance and so on. To keep the computational effort and time low, the models used in the design tool need to be simple and fast to execute, yet sufficiently precise and accurate. When dealing with medium voltage, bulk power conversion, special attention needs to be paid to correct insulation in order to prevent damage and component failure. Furthermore, thermal coordination, i.e. constraints regarding operational temperatures, is another important limiting factor for transformer design, therefore it is crucial to be able to estimate their distributions correctly. This paper introduces the thermal-hydraulic model (THM) which determines the oil temperature distribution and the average volume flows, useful for modeling and thermal coordination of the MFT designs with oil-immersed windings.

Figure 1 shows the considered core-type MFT concept, envisioned as an integral part of a 1MW rated DC-DC converter, which uses integrated gate-commutated thyristors as switching devices, owing to their high current ratings and low conduction losses [3]. Nevertheless, due to processing of high powers the semiconductor switches are cooled with deionized (DI) water which provides an opportunity to use the same cooling system for the MFT. Therefore, the transformer windings are designed in the form of hollow conductors which allow for internal water cooling. Additionally, the windings are immersed in oil which positively affects the overall power density of the transformer, due to reduced required insulation distances. Thereby, the primary and secondary windings are placed in pairs concentrically around each of the core limbs. With the cold water entering the windings at the top of each vessel (marked with blue arrows in Figure 1) and exiting with an increased temperature at the bottom (marked with red arrows), a temperature gradient is formed along the windings in the vertical direction. Consequently, a variable volumetric flow of the coolant (DI water) directly influences the temperature gradient value. Note that while DI water is selected as the main cooling method for the windings, the paper focuses on the thermal problem inside of the oil vessel and not inside the hollow conductors. As a consequence of the vertical temperature gradient and together with the winding excess loss, i.e. a small fraction of the total winding losses

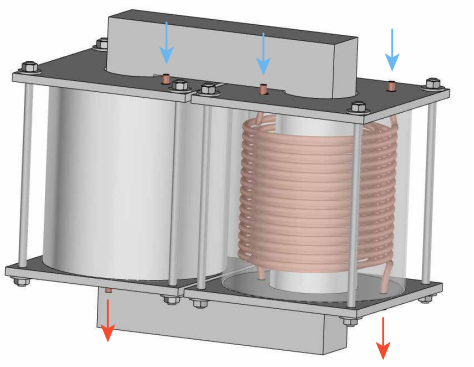

Figure 1: MFT concept with two oil vessels.

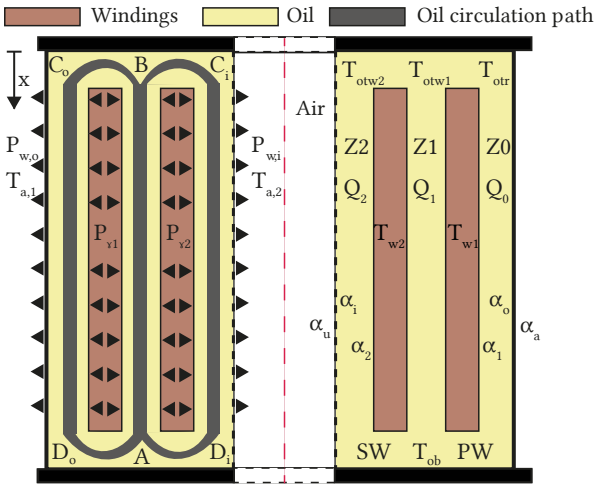

Figure 2: 2D front view of the oil vessel with simplified foil windings.

which did not get exchanged internally with the water, natural oil circulation is achieved.

Models similar to THM have been already developed for large distribution power transformers with different types of oil cooling (oil direct (OD), oil natural (ON)) and mostly disc transformer windings, as presented in [4]–[6]. Apart from large power transformers which are fully immersed in oil, the authors have not found further relevant references to related models. One of the key differences compared to the existing models, however, is the fact that for large power transformers the oil is used not only for its insulation capabilities, but also to provide adequate cooling. As previously mentioned, in the work presented in this paper, the oil is mainly selected to provide insulation and increase power density, but also due to its self-healing properties which are of crucial importance in case of partial discharges.

II. Thermal-hydraulic Model

The presented model is of analytical nature and it consists of two parts: 1) the thermal part which deals with heat exchange phenomenon following the principles of conservation of heat and mass; 2) the hydraulic part of the model which is determined based on the pressure equilibrium established in identified closed loops in which oil circulates. For both model parts laminar oil flow is assumed and only the steady-state operation is considered. The helical coil windings, designed initially with hollow conductors, are approximated with foil windings in order to simplify the model derivation.

Figure 2 illustrates the 2D cross-sectional axis-symmetric front view of a single oil vessel containing the simplified winding representations. The axis of symmetry is presented by the red dashed line in the middle. The left and the right vessel side in Figure 2 show different parameters relevant for the THM, nevertheless, the two sides are exactly symmetrical. Thereby, the secondary winding (SW) is set closer to the inner tube of the vessel (occupied by the core limb, which is not explicitly shown, and the surrounding air) and it assumes an average temperature T_{w2}, whereas the primary winding (PW) is placed concentrically around the SW, closer to the outer vessel wall with an average winding temperature T_{w1}. The two temperatures are determined based on the copper temperatures measured or estimated at the top and at the bottom of the conductors once they exit the oil vessel. Due to winding losses in the steady state PW and SW release in their surrounding the losses $P_{\gamma 1}$ and $P_{\gamma 2}$, respectively. The exact loss values are derived from the total winding losses by estimating the percentage that did not get exchanged with DI water applied internally for the cooling of the conductors. The estimation is based on the DI water temperature data entering and exiting the winding, as well as the information about the injected losses. Moreover, the model considers two different ambient temperatures, $T_{\mathrm{a,1}}$ and $T_{\mathrm{a,2}}$, which correspond to the air temperature outside the oil vessel and inside its inner tube. As illustrated in Figure 1 in case of a functional MFT, the inner space of the vessel is occupied by a core limb, which is expected to have increased temperature due to core losses. Furthermore, the model is able to consider exact winding arrangements inside of the vessel, so that different insulation distances are included which enables the MFT design optimization tool to consider the geometry impact on the oil temperature and velocity distribution.

According to Figure 2 two distinct oil paths can be observed: ABC_oD_oA and ABC_iD_iA. The points A, B, C_i, C_o, D_i and D_o are selected as characteristic points in which the oil temperature is of interest. In fact, points A, D_i and D_o belong to concentric circles (when observed in 3D) positioned vertically at the half distance between the bottom of the windings and the bottom vessel lid. In horizontal direction (perpendicular to the figure plane) the concentric circles are placed between PW and SW (A) and the pairs of outer vessel wall and PW (D_o) and the inner vessel wall and SW (D_i), respectively, as illustrated in Figure 3. To simplify the model derivation it is assumed that the oil temperatures at the three concentric circles are identical and correspond to T_{ob}. The same logic is followed for the points B, C_i and C_o at the top of the windings, however, it is assumed that the oil temperatures vary and they agree with T_{otw1}, T_{otw2} and T_{otr}, respectively. Three cylindrical zones of oil circulation Z_0, Z_1 and Z_2 are marked in Figure 3 together with the direction of oil movement for each of the zones. Note that the color legend given in Figure 2 applies to Figure 3 as well.

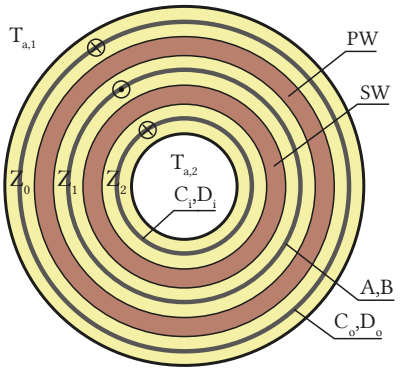

Figure 3: 2D top view of the oil vessel with simplified foil windings.

The oil in zone 1 (Z_1), heated from the excess PW and SW losses ($P_{\gamma 1}$ and $P_{\gamma 2}$), experiences mass density decrease, i.e. volume expansion and rises from A to B (average volumetric flow Q_1) due to buoyancy forces. At the top oil starts to cool down, becoming heavier, owing to lower winding temperatures compared to the bottom winding parts, which is achieved by the temperature gradient due to the present water cooling. At this point the oil splits into two paths C_oD_o (zone Z_0, flow Q_0) and C_iD_i (zone Z_2, flow Q_2), where it continues cooling at the outer and inner vessel wall through natural convection and returns down to point A, where the process of oil heating starts again. Thereby, the heat exchanged with the vertical vessel walls is denoted with $P_{\text{w,o}}$ and $P_{\text{w,i}}$, for the outer and the inner vessel wall, respectively. Moreover, a horizontal heat exchange is considered as well, marked with $P_{\text{h,t}}$ and $P_{\text{h,b}}$, corresponding to the top and bottom vessel lid. Furthermore, note that the presented model is developed for the steady state transformer operation, and it is not able to estimate oil temperatures and velocities during transient states.

A. Thermal Part of THM

Energy balance equations established for each of the oil zones are given in (1)-(6), with w_0, w_1 and w_2 as the respective average oil velocities, and A_0, A_1 and A_2 as the horizontal cross sections for each of the zones. Thereby, it is assumed that total excess winding losses ($P_{\text{tot}} = P_{\gamma 1} + P_{\gamma 2}$) that are exchanged with the oil get evacuated both at the vertical and horizontal vessel walls. Nevertheless, the horizontal heat exchange, in regions AD_i, AD_o and BC_i, BC_o is significantly smaller compared to the heat exchanged vertically, i.e. between the windings, and the inner and outer vessel wall. Additionally, it is assumed that the excess PW and SW heat losses are distributed between the respective zones (Z_0-Z_1 and Z_1-Z_2) according to ratio parameters z and y. The horizontal heat exchange ($P^A_{\text{h,b}}$ at the bottom, $P^A_{\text{h,t}}$ at the top) between oil and the surrounding air is distributed across the zones by the respective horizontal cross sections (A). Finally, it is assumed that the air temperature at the top and bottom of the vessel takes the same values as $T_{\text{a,1}}$. The energy balance equations defined for the three oil zones are given below.

Zone 0:

$$zP_{\gamma 1} - P_{\text{w,o}} - P^{A_0}_{\text{h,t}} - P^{A_0}_{\text{h,b}} = \rho c_p Q_0 (T_{\text{otr}} - T_{\text{ob}}), \quad (1)$$

$$Q_0 = A_0 w_0, \quad P^{A_0}_{\text{h,b/t}} = A_0 k^h_p (T_{\text{ob/otr}} - T_{\text{a,1}}) \quad (2)$$

Zone 1:

$$(1-z)P_{\gamma 1} + (1-y)P_{\gamma 2} - P^{A_1}_{\text{h,t}} - P^{A_1}_{\text{h,b}} = \rho c_p Q_1 (T_{\text{otw1}} - T_{\text{ob}}), \quad (3)$$

$$w_1 = \frac{1}{A_1} \underbrace{(Q_0 + Q_2)}_{=Q_1}, \; P^{A_1}_{\text{h,b/t}} = A_1 k^h_p (T_{\text{ob/otw1}} - T_{\text{a,1}}) \quad (4)$$

Zone 2:

$$yP_{\gamma 2} - P_{\text{w,i}} - P^{A_2}_{\text{h,t}} - P^{A_2}_{\text{h,b}} = \rho c_p Q_2 (T_{\text{otw2}} - T_{\text{ob}}), \quad (5)$$

$$Q_2 = A_2 w_2 \quad P^{A_2}_{\text{h,b/t}} = A_2 k^h_p (T_{\text{ob/otw2}} - T_{\text{a,1}}) \quad (6)$$

Parameters ρ and c_p give the oil density and its specific heat capacity at oil temperature T_{ob}. Note that the average oil velocity w_1 in zone Z_1 is determined by the other two average oil velocities w_0 and w_2, due to the assumption that the oil flowing through Z_1 gets split into the flows of the zones Z_0 and Z_1.

The goal of the THM is to correctly estimate characteristic oil temperatures depending on the operating point of the MFT and of the water cooling unit (WCU), i.e. the amount of winding losses and the characteristics of the DI water entering the windings, respectively. In the model the WCU operating point is represented by the volumetric flow of DI water and the inlet water temperature. The outlet water temperature depends on the amount of dissipated winding losses. The following equation determines the amount of losses absorbed by the flowing DI water

$$P_{DI,w} = \dot{m} c_p \Delta T_w, \quad (7)$$

with $\dot{m}$ as the volumetric flow of cooling DI water, c_p as its specific heat capacity and ΔT_w as the water temperature increase from the bottom to the top due to winding loss absorption. Considering the total amount of winding loss and the previous equation, the excess PW and SW losses $P_{\gamma 1}$ and $P_{\gamma 2}$ can be estimated. At this moment in time the authors have not developed a model for estimating the outlet water temperature based on the amount of losses dissipated in the windings. Therefore, this specific information is collected directly from experimental measurements of oil, DI water and copper temperatures. The experimental characterization of the model is given in Section III.

The cooling powers along the vertical vessel walls are obtained by integration

$$P_{\text{w,o}} = \int_0^H (T_{o,0}(x) - T_{a,1}) k^o_p O^o dx = \frac{A_o}{A_i + A_o} P_{\text{diff}}, \quad (8)$$

$$P_{\text{w,i}} = \int_0^H (T_{o,2}(x) - T_{a,2}) k^i_p O^i dx = \frac{A_i}{A_i + A_o} P_{\text{diff}}, \quad (9)$$

$$P_{\text{diff}} = P_{\text{tot}} - P^{A_0+A_1+A_2}_{\text{h,b}} - P^{A_0+A_1+A_2}_{\text{h,t}}, \quad (10)$$

where H is the vertical height of the oil in the vessel, A_o, A_i are the vertical surfaces of the outer and inner vessel wall, respectively.

At this point, it is assumed that the difference between the total excess winding losses (P_{tot}) and the horizontally exchanged heat are distributed across the vertical vessel walls based on the simple proportion of vessel wall surfaces that take part in the heat exchange process. Further, $T_{o,0}(x)$ and $T_{o,2}(x)$ represent vertical oil temperature distributions for the outer and inner oil zones (Z_0 and Z_2), O^o and O^i are the circumferences of the outer and inner vessel wall, respectively. This further implies the assumption that all the oil points in a horizontal layer at a certain height assume the same temperature, zone-wise, i.e. in concentric annulus rings as given in Figure 3. The

coefficients k_p^o and k_p^i are the total heat transfer coefficients (HTCs) determined by the following equations

$$k_p^o = \frac{1}{\frac{1}{\alpha_o} + \frac{\delta_w}{\lambda_w} + \frac{1}{\alpha_a}},\ k_p^i = \frac{1}{\frac{1}{\alpha_u} + \frac{\delta_w}{\lambda_w} + \frac{1}{\alpha_i}},\ \alpha = \overline{\mathrm{Nu}}\frac{\lambda_m}{L} \quad (11)$$

with α as the convection HTC between a certain surface and the passing fluid, and λ_w, δ_w as the thermal conductivity and the thickness of the vertical vessel wall. Thereby, α_u, α_a and α_i, α_o in pairs give the HTCs for the convective heat transfer between the inner and the outer vessel wall in pair and the surrounding air and oil, respectively. HTCs α_1 and α_2 characterize accordingly the heat transfer between the oil and PW and SW, as denoted in Figure 2. Relations similar to (11) hold for the total HTC k_p^l which describes the convective heat exchange between the oil and the surrounding air at the top and bottom horizontal surface of the vessel. The introduced convection HTCs, which eventually define the total HTC value, can be determined with the help of known average Nusselt correlations ($\overline{\mathrm{Nu}}$) obtained for natural convection in laminar regime [7], [8], the medium's thermal conductivity λ_m and the characteristic length L which participates in the convective heat transfer process. Each of the correlations depends on the medium specifications and the geometrical arrangement through which the fluid is passing (e.g. tall vertical enclosure with uniform heat flux on the sidewalls, vertical cylinder with isothermal surfaces and so on). Nevertheless, due to geometric specificity of the existing empirically determined Nusselt correlations, which do not exactly match the geometry of the considered oil vessel given in Figure 2, the total HTCs k_p^o, k_p^i and k_p^l and the convective HTCs α_1 and α_2 are determined for model purposes with the help of a genetic algorithm, explained in Section II-C.

The vertical oil temperature distributions are determined with the help of following differential equations of energy balance

$$(k_p^i O^i(T_{o,2}(x) - T_{a,2}) + \alpha_2 O_2(T_{o,2}(x) - T_{\mathrm{w2}}))dx = \quad (12)$$
$$= \rho c_p Q_2 dT_{o,2}(x),$$

$$(k_p^o O^o(T_{o,0}(x) - T_{a,1}) + \alpha_1 O_1(T_{o,0}(x) - T_{\mathrm{w1}}))dx = \quad (13)$$
$$= \rho c_p Q_0 dT_{o,0}(x),$$

with O_1 and O_2 as the outer and inner circumference of the primary and the secondary winding, respectively. Once the solutions to oil temperature distributions in the x direction are derived, they are applied to equations (8)-(10).

Eventually, with the help of statistical software package Maple and based on the equations (1)-(13) four analytical expressions for four distinct oil temperature points (T_{otr}, T_{otw1} and T_{otw2} selected at the top of zones Z_0, Z_1 and Z_2, respectively, and T_{ob} as the homogeneous bottom oil temperature) are derived, which depend on the average oil velocities w_0 and w_2, among other parameters.

B. Hydraulic Part of THM

For the second part of the model it is assumed that only a single oil phase exists, the oil passages have smooth walls and that the flow is stabilized and in laminar regime. Due to the fact that the expressions for hydraulic resistances are derived (exclusively) for the case of forced convection [9], where a certain condition related to the Reynolds number needs to be fulfilled, for this THM part it is assumed that oil takes part in forced convective heat transfer. This assumption is not far from being valid if the existing buoyancy force is considered.

As a consequence of oil density change, a thermal driving force, i.e. buoyancy force, is created which causes oil circulation and produces pressure [10]. A general expression for the produced pressure is given in (14) and adjusted to the specific oil path geometry, shown in Figure 2, in (15):

$$p_{\mathrm{T}} = \rho g \beta \Delta T_o \Delta H \quad \Rightarrow \quad (14)$$

$$\Rightarrow \quad p_{\mathrm{T}} = \rho g \beta \left(\frac{1}{2} T_{ot} - T_a + \frac{1}{2} T_{ob} - \Delta T_{o-a} \right) \quad (15)$$

Thereby, parameter β is the volume expansion coefficient, g is the gravity vector, ΔT_o stands for the vertical temperature gradient ($\Delta T_o = T_{\mathrm{ot}} - T_{\mathrm{ob}}$), whereas ΔH is the corresponding height difference. Note that the temperature T_{ot} can assume any of the two top temperatures, T_{otr} or T_{otw2}, depending on the considered oil circulation path, ABC_oD_oA or ABC_iD_iA, respectively. Temperature ΔT_{o-a} is known as the logarithmic mean temperature difference and it is defined by the following relation

$$\Delta T_{o-a} = \frac{T_{\mathrm{ot}} - T_{\mathrm{ob}}}{\ln(T_{\mathrm{ot}} - T_a) - \ln(T_{\mathrm{ob}} - T_a)}, \quad (16)$$

with T_{a} as one of the two ambient temperatures, $T_{\mathrm{a,1}}$ and $T_{\mathrm{a,2}}$, depending again on the considered oil loop.

On the other hand, oil streaming causes dispersed and local pressure drops. The latter type occurs in elements where the oil changes the streaming direction, such as in cases of confluence and branching. Compared to the first type of pressure drops, it can be neglected. The first type, also known as the frictional pressure drop, is characteristic for flows through elements with constant cross sections and it is determined by a pressure drop coefficient ξ. The value of the coefficient depends on the flow type and the geometry of oil passages, as well as the oil density and average velocity [9], as given by the following relations

$$\Delta p = \xi \frac{\rho w^2}{2} \quad \Rightarrow \quad \xi = \lambda \frac{l}{D_h}, \quad \text{with} \quad (17)$$
$$\lambda = k_{\text{non-c}} \frac{64}{\mathrm{Re}} \quad \text{and} \quad \mathrm{Re} = w \frac{D_h}{\nu}.$$

Parameter λ gives the friction coefficient and it is determined by the smoothness of the oil passage walls and by the flow type, l is the conduit length, D_h is the hydraulic diameter and Re is the Reynolds number. In order for the assumption of laminar flow to be correct, the Reynolds number needs to have a value below 2000. The parameter $k_{\text{non-c}}$ is the correction factor for non-standard conduit shapes, since in the specific case illustrated in Figure 2 the oil flows through concentric annuluses of circular tubes [9].

Eventually, a steady state and stabilized oil flows are reached when the pressure equilibrium holds for each of the two oil

loops, i.e. once the produced pressure matches the pressure drops caused due to oil movement. The sought equilibrium is finally expressed by the following relations

$$p_{\text{eq,o}}: \; p_{\text{T},ABC_oD_oA} = \Delta p_1 + \Delta p_0, \tag{18}$$

$$p_{\text{eq,i}}: \; p_{\text{T},ABC_iD_iA} = \Delta p_1 + \Delta p_2, \tag{19}$$

with Δp_0, Δp_1 and Δp_2 describing the pressure drops in zones Z_0, Z_1 and Z_2, respectively, calculated based on (17). The left-hand side of the pressure balance equation is determined based on (14)-(16). Note that the pressures produced and lost in the horizontal parts of the two main oil paths (BC_o, BC_i, AD_o, AD_i) are not considered. This second part of THM provides another two model-relevant equations which describe the pressure equilibrium of the two main oil loops, and they are coupled with the four characteristic oil temperatures and the two relevant average oil velocities.

C. THM Implementation

To summarize, the developed analytical model consists of four expressions for oil temperatures and two relations describing the pressure balance in the main oil loops. Due to complexity of the considered heat transfer system and existing uncertainty of accurate analytical modeling of heat transfer phenomena inside of the oil vessel, a set x of 9 parameters, defined in Table I, is considered optimizable within certain boundaries. The optimal parameters are determined based on the collected experimental thermal measurements (presented in Section III) and with the help of multi-objective optimization. The main idea is that the selected optimization algorithm can minimize the difference between the measured and the analytically obtained oil temperature values, while respecting the pressure equilibrium, and for a certain optimal set of parameters. The optimization process can be described as:

$$\underset{x}{\text{minimize}} \quad f(x), g(x) \tag{20}$$

$$\text{subject to} \quad B_l \leq x \leq B_h \tag{21}$$

Table I: Set x of selected optimizable parameters.

Parameter	Description
w_0	average oil velocity in zone Z_0
w_2	average oil velocity in zone Z_2
k_p^o	total HTC describing the exchange between the air (T_{a1}) and oil at the outer vessel wall
k_p^i	total HTC describing the exchange between the air (T_{a2}) and oil at the inner vessel wall
k_p^l	total HTC between the air (T_{a1}) and oil at the bottom and top vessel lid
z	ratio of $P_{\gamma 1}$ that heats the oil in zone Z_0
y	ratio of $P_{\gamma 2}$ that heats the oil in zone Z_2
α_1	convective HTC describing the exchange between the oil in zone Z_0 and PW
α_2	convective HTC describing the exchange between the oil in zone Z_2 and SW

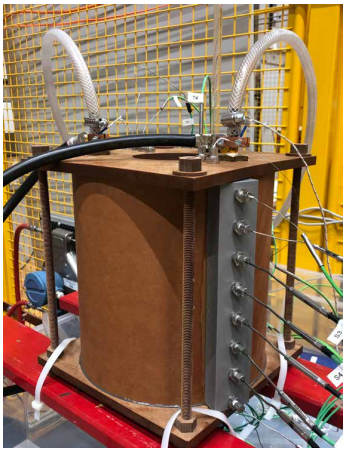

Figure 4: Vessel, instrumented with thermocouples, containing oil and a pair of PW and SW connected to a DC power source and DI WCU.

The respective objective functions are defined as:

$$f(x) = \sum_{i=\text{otr,otw1,otw2,ob}} |T_i(x) - T_i^*| \tag{22}$$

$$g(x) = |p_{\text{eq,o}}(x) + p_{\text{eq,i}}(x)| \tag{23}$$

Note that the asterisk sign stands for the experimentally obtained oil temperatures and the variable x corresponds to the parameter set $\{w_0, w_2, z, y, k_p^o, k_p^i, k_p^h, \alpha_1, \alpha_2\}$. The two sets B_l and B_h give the lower and upper constraints of the selected parameters.

In order to maximize the probability of finding global minima, the implementation method is based on genetic algorithms [11]. An additional advantage of this specific method is that no initial conditions are required. Moreover, with appropriate selections of population size and number of iterations, it is ensured that the algorithm maximizes the diversity of the populations between consecutive generations.

III. THM Characterization and Results

The experimental measurements necessary for the characterization of THM are collected with the help of a down-scaled test setup shown in Figure 4. The setup consists of a single oil vessel made of paper-phenolic material containing a set of PW and SW hollow conductors with fixed interwinding distance and filled with synthetic ester dielectric oil (Midel 7131). In the given test setup both windings have 15 turns and a turn-to-turn distance of 3 mm. The external diameter of the hollow conductor profile is 8 mm, whereas the wall thickness is 1.4 mm. In order to measure various oil temperatures,= 18 thermocouples (TCs) are placed in the same vertical plane which passes through the vessel center. Five TCs are placed in the same horizontal line at the vessel top (marked with $T_1 - T_5$) and five at the bottom (marked with $B_1 - B_5$), measuring the temperatures at the center of each zone (Z_0, Z_1 and Z_2). The remaining eight TCs (denoted with $S_1 - S_8$) are inserted equidistantly on the vessel side exactly between the outer vessel wall and the PW, as shown in Figure 4. To observe the conductor temperatures and determine the average values of T_{w1} and T_{w2}, another four TCs are attached to the

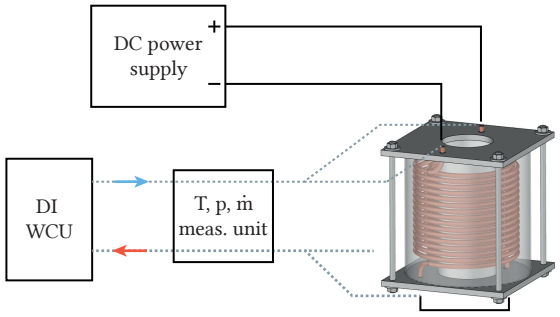

Figure 5: Schematics of: electrical connections between PW and SW (in series) and a DC power supply, marked by black lines; DI water hoses distributing cold water to the top of the windings (in parallel) and collecting back the warm water from the bottom; marked with grey dashed lines.

top and bottom parts of the windings directly outside of the oil vessel. Furthermore, black cable connections from Figure 4 provide controlled direct current to PW and SW connected in series, in order to imitate losses present during transformer operation. Additionally, the transparent hoses supply the windings with DI water from a WCU of controlled temperature and volumetric flow. Figure 5 provides a schematic of the winding connections to the DC power source and the WCU. Additional setup (marked with T, p, $\dot{m}$ meas. unit) is assembled in order to measure temperature, pressure and volumetric flow of the incoming and outgoing cooling water. The above described setup was used to collect measurements for various operating points. Thereby, the current of the DC source was varied in the range of 250 A − 450 A with a 20 A step, which corresponds to 11 measurements with roughly 1 kW − 3 kW of total winding losses. This range of losses corresponds to the available winding loss budget for a 1 MW MFT design. The volumetric flow of the DI water was set to approximately 22.5 mL s^{-1}.

Figure 6 gives an example of recorded oil temperature distributions for the operating point of 420 A, which corresponds to approximately 2.9 kW of losses. By observing the obtained temperature forms for differently placed thermocouples and based on the magnified view of the steady-state temperatures, one can make presumptions regarding the oil movement. Temperature forms recorded at the top of the vessel exhibit higher oscillations than the side or the bottom measurements, which corresponds to the fact that the oil is surging up towards the vessel top with elevated temperature and circulating back to the bottom while being cooled at the outer and inner vessel walls. Moreover, the selection of a single characteristic bottom oil temperature compared to the three distinct top temperatures confirms to be correct, considering the temperature span of the respective thermocouple groups.

To obtain the four characteristic oil temperatures (T^*_{ob}, T^*_{otr}, T^*_{otw1} and T^*_{otw2}) from the collected measurements the averaging of steady-state temperatures is carried out as:

$$T^*_{\text{ob}} = \text{avg}(B_1, B_2, B_3, B_4, B_5, S_8),\ T^*_{\text{otr}} = \text{avg}(T_1, S_1), \quad (24)$$

$$T^*_{\text{otw1}} = \text{avg}(T_2, T_5), \quad T^*_{\text{otw2}} = \text{avg}(T_3, T_4) \quad (25)$$

Finally, Figure 7 compares the results obtained when the THM is used to estimate oil temperatures for various operating points with the recorded measurements, and shows an overall

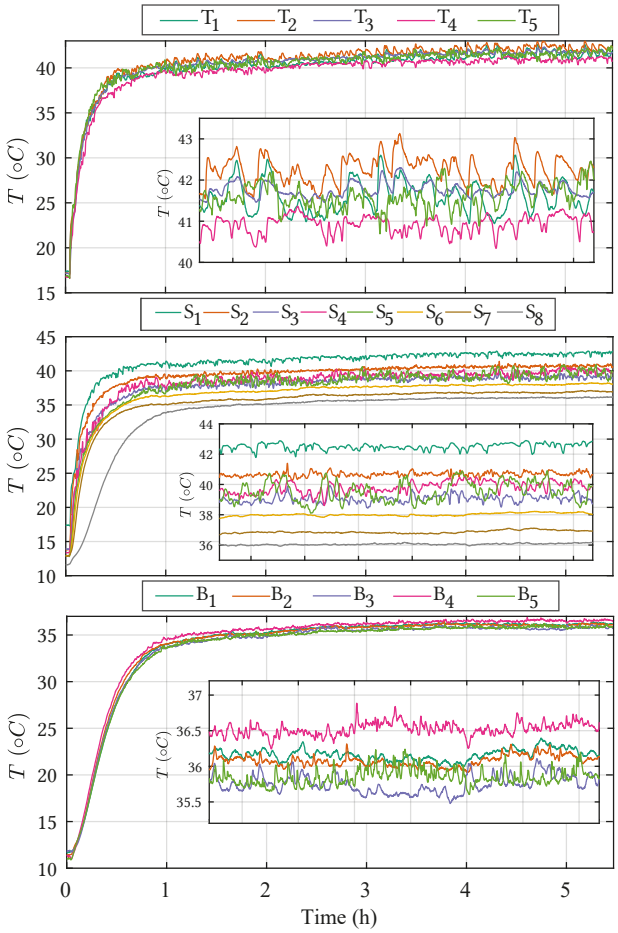

Figure 6: Oil temperature measurements taken at the top (T_1 - T_5), on the side (S_1 - S_8) and at the bottom (B_1 - B_5) of the vessel for the operating point of 420 A. The magnified view for each plot gives the corresponding steady-state temperatures at the end of the recording time.

good agreement between the two. The highest deviation can be generally observed for estimation of the bottom oil temperature T_{ob} and it reaches the peak at 4.2 °C for the 310 A DC operating point. Furthermore, the accuracy of the THM improves significantly with higher winding losses, where the deviation from the measured for all four estimated temperatures, in case the same operating point is observed, remains very small. Due to the fact that the average oil velocities are eventually determined by the genetic algorithm and due to the current inability to experimentally measure these values, as well as due to the complexity of such an experiment, the velocities obtained from the analytical model are not explicitly presented. Nevertheless, for all the considered operating points they remain in the range of several millimeters per second.

IV. Conclusion

This paper presented an analytical model for characteristic oil temperature estimations, especially relevant for MFTs with oil-immersed windings. Due to the fact that heating of the oil causes its movement, which further gives rise to pressure drops, both thermal and hydraulic sides of the problem need to be considered for correct and accurate temperature estimation. Nevertheless, due to the complexity of analytical modeling of

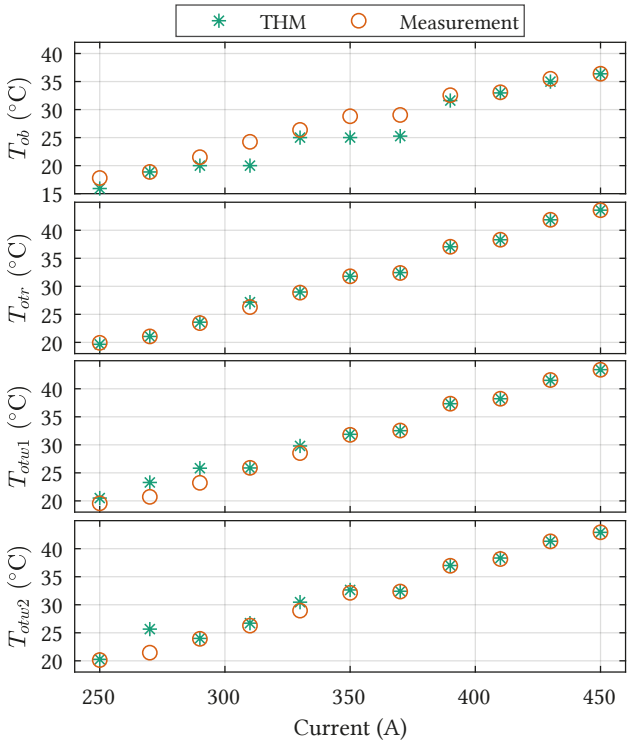

Figure 7: Comparison of experimentally obtained oil temperature measurements with the analytical THM results for various operating points.

heat transfer phenomena combined with fluid dynamics, the introduced model had to be additionally characterized with the help of experimental temperature measurements and an optimization algorithm. Finally, good agreement is achieved between the measured characteristic oil temperatures and the THM results for various operating points.

The developed model is of significant importance for the thermal coordination of a design and it provides useful inputs to the overall steady-state thermal model of the MFT. However, due to the complexity of its current implementation it cannot directly be included in the first layer of the MFT design process, where millions of potential designs need to be evaluated fast. Nonetheless, as already mentioned, it can serve well to aid and verify the overall thermal image of MFT designs with oil-immersed windings.

Acknowledgment

The results presented in this paper are a part of the EMPOWER project that has received funding from the European Research Council (ERC) under the European Union's Horizon 2020 research and innovation programme (Grant agreement No. 818706).

References

[1] J. E. Huber and J. W. Kolar, "Solid-state transformers: On the origins and evolution of key concepts", *IEEE Industrial Electronics Magazine*, vol. 10, no. 3, pp. 19–28, 2016.

[2] G. Ortiz, "High-power dc-dc converter technologies for smart grid and traction applications", Ph.D. dissertation, ETH Zurich, 2014.

[3] D. Stamenković, U. R. Vemulapati, T. Stiasny, M. Rahimo and D. Dujić, "IGCT low-current switching - tCAD and experimental characterization", *IEEE Transactions on Industrial Electronics*, vol. 67, no. 8, pp. 6302–6311, 2019.

[4] A. Oliver, "Estimation of transformer winding temperatures and coolant flows using a general network method", in *IEE Proceedings C (Generation, Transmission and Distribution)*, IET, vol. 127, 1980, pp. 395–405.

[5] J. Zhang and X. Li, "Oil cooling for disk-type transformer windings-part 1: Theory and model development", *IEEE Transactions on Power Delivery*, vol. 21, no. 3, pp. 1318–1325, 2006.

[6] Z. R. Radakovic and M. S. Sorgic, "Basics of detailed thermal-hydraulic model for thermal design of oil power transformers", *IEEE Transactions on Power Delivery*, vol. 25, no. 2, pp. 790–802, 2010.

[7] A. Bejan, *Convection heat transfer*. John wiley & sons, 2013.

[8] F. P. Incropera, A. S. Lavine, T. L. Bergman and D. P. DeWitt, *Fundamentals of heat and mass transfer*. Wiley, 2007.

[9] I. E. Idelchik, "Handbook of hydraulic resistance", *Washington*, 1986.

[10] K. Karsai, D. Kerényi and L. Kiss, "Large power transformers", 1987.

[11] J. H. Holland, "Genetic algorithms and adaptation", in *Adaptive Control of Ill-Defined Systems*, Springer, 1984, pp. 317–333.